To link to this article : doi: 10.1016/j.jcat.2015.01.009
URL : http://dx.doi.org/10.1016/j.jcat.2015.01.009

To cite this version : Cardozo, Andrés Fernando and Julcour-Lebigue, Carine and Barthe, Laurie and Blanco, Jean-François and Chen, Si and Gayet, Florence and Manoury, Eric and Zhang, Xuewei and Lansalot, Muriel and Charleux, Bernadette and D'Agosto, Franck and Poli, Rinaldo and Delmas, Henri Aqueous phase homogeneous catalysis using core–shell nanoreactors: Application to rhodium-catalyzed hydroformylation of 1-octene. (2015) Journal of Catalysis, vol. 324. pp. 1-8. ISSN 0021-9517

Aqueous phase homogeneous catalysis using core–shell nanoreactors: Application to rhodium-catalyzed hydroformylation of 1-octene

Andrés F. Cardozo [a,c], Carine Julcour [a,c,*], Laurie Barthe [a,c], Jean-François Blanco [a,c], Si Chen [b,c], Florence Gayet [b,c], Eric Manoury [b,c], Xuewei Zhang [d], Muriel Lansalot [d], Bernadette Charleux [d,e], Franck D'Agosto [d], Rinaldo Poli [b,c,e], Henri Delmas [a,c]

[a] CNRS, LGC (Laboratoire de Génie Chimique), 4 Allée Emile Monso, BP 84234, 31432 Toulouse Cedex 4, France
[b] CNRS, LCC (Laboratoire de Chimie de Coordination), 205 route de Narbonne, BP 44099, 31077 Toulouse Cedex 4, France
[c] Université de Toulouse, INPT, UPS, Toulouse, France
[d] Université de Lyon, Univ. Lyon 1, CPE Lyon, CNRS, UMR 5265, C2P2 (Chemistry, Catalysis, Polymers & Processes), Team LCPP Bat 308F, 43 Bd du 11 Novembre 1918, 69616 Villeurbanne, France
[e] Institut Universitaire de France, 103, bd Saint-Michel, 75005 Paris, France

A B S T R A C T

High catalytic activity (turnover frequencies up to 700 h^{-1}) was achieved using new triphenylphosphine-functionalized core cross-linked micelles, TPP@CCM, as nanoreactors and $[Rh(acac)(CO)_2]$ as catalyst precursor for the aqueous biphasic hydroformylation of 1-octene. While the hydrophobic core of the polymer offers an adequate environment for the catalytic reaction, its hydrophilic shell confines the catalyst into the aqueous phase and prevents extensive leaching toward the substrate/product phase. Selectivity is better than that of the homogeneous reaction catalyzed by the Rh/PPh_3 system, with minor isomerization and linear to branched aldehyde ratios (l/b) between 3 and 6. Various operating parameters, such as catalyst/ligand concentration, temperature, and P/Rh ratio, were varied and proved that these nanoreactors do not suffer from significant mass transfer limitations. The effect of the nanoreactor hydrophobic core size and degree of functionalization on activity and on l/b regioselectivity has also been investigated. The possible causes of catalyst leaching are discussed.

Keywords:
Biphasic catalysis
Catalyst immobilization
Core–shell polymer
Cross-linked micelle
Rhodium
Hydroformylation

1. Introduction

Biphasic catalysis is an elegant strategy of catalyst immobilization in which the catalyst is confined into a solvent slightly miscible or immiscible with the products, allowing fast separation of the catalytic phase by settling and easy recycling. Although there has been increasing research on the application of biphasic reaction media with innovative solvents—such as fluorous solvents [1] and ionic liquids [2,3]—yielding successful developments like the Difasol process [4], use of water to solubilize the catalyst has the advantage of driving the system toward sustainability and diminishing costs. A well-established industrial application of the aqueous biphasic catalysis is the Ruhrchemie/Rhône Poulenc oxo process, in which propene is converted to butanal by a hydrosoluble rhodium complex. However, the same process cannot be applied to longer chain olefins (>C4), their poor solubility in water leading to poor reaction rates. Many strategies have been developed to overcome this issue, among which use of cosolvents [5–7] or phase transfer agents such as cyclodextrins [8,9] or activated carbons [10]. On the other hand, surfactants or amphiphilic ligands can also create organic substrate-rich nano-objects (micelles) within the aqueous catalyst phase. The latter yield more stable and more adequately tunable catalytic systems, but still the dynamic structure of the micelles results in catalyst loss at the interface and may also generate stable emulsions by excessive swelling of the micellar core [11,12]. In a novel approach recently introduced by us [13], both limitations have been removed by turning the self-organized and dynamic micellar architecture into a unimolecular polymeric core–shell nano-object by cross-linking the hydrophobic segments of self-assembled amphiphilic block copolymers. Hence, swelling of these particles is limited by the dimensions of the resulting macromolecule and the micellar equilibrium with the free arms is removed.

A few examples of unimolecular macrostructures that achieve a favorable environment for efficient catalysis in water are available in the open literature, yet with various architectures

* Corresponding author at: CNRS, LGC (Laboratoire de Génie Chimique), 4 Allée Emile Monso, BP 84234, 31432 Toulouse Cedex 4, France.
E-mail address: carine.julcour@ensiacet.fr (C. Julcour).

http://dx.doi.org/10.1016/j.jcat.2015.01.009

and levels of complexity. Using natural polyphenols as amphiphilic ligands, Mao et al. [14] could prepare noble metal complex and noble metal nanoparticle catalysts for the biphasic hydrogenation of cinnamaldehyde and quinoline. The authors observed some decrease of conversion upon recycling, whose extent depended on the content of polyphenols: from 61% to 97% of the original activity was retained after five runs. Gong et al. [15] synthesized four water-soluble dendritic phosphonated ligands starting from poly(amido amine) (PAMAM) dendrimers. The first ligand resulted from a partial functionalization of the dendritic surface with monophosphine moieties, the remaining amine functions enabling its dissolution into the aqueous phase. They also alternated phosphine and sulfonate functions to further increase phosphine loading while keeping enough water solubility. Finally, they grafted some long aliphatic chains to better interact with the olefin and enhance its solubilization into the aqueous phase. These various objects thus comprised a limited amount of phosphorus atoms (18 maximum per object), mainly located at the periphery. Their application to the hydroformylation of 1-octene led to relatively low turnover frequency (TOF) values (<25 h^{-1}) and significant loss of rhodium, as indicated by the yellow coloring of the organic phase. Terashima et al. [16] proposed a different approach to incorporate monophosphine units into a star polymer, using controlled radical polymerization mediated by ruthenium. As the result of the simultaneous introduction of phosphine monomer, amphiphilic macroinitiator, and cross-linking agent, the phosphine ligands were here confined within the obtained polymer microgel core, entrapping ruthenium. These objects were successfully tested for Ru-catalyzed hydrogenation under a thermomorphic approach [17]. In a close strategy of catalyst confinement, Weck et al. [18] prepared shell cross-linked micelles containing catalytic Co(III) salen functions in the hydrophobic cores from amphiphilic triblock polymers. Applied to the hydrolytic kinetic resolution of epoxides, these catalysts exhibited substrate selectivity based on hydrophobicity, unlike their non-cross-linked analogs. They could also be successfully recycled eight times by ultrafiltration. L-Proline functionalized poly(methyl methacrylate) (PMMA) nanogel particles were also proposed by O'Reilly et al. [19] as catalysts for aldol reactions in water. An increase in the weight percentage of L-proline methacrylate incorporated in the nanogel particles from 2% to 10% strongly reduced their activity, while changes in the cross-linking density (CLD) in the 0.5–5 wt% range had only a minor effect. CLD as high as 50 wt% was indeed required to shut down the reaction. Moreover, the more hydrophobic the nanogel core, the higher the observed enantioselectivity. These examples prove that the performance and stability of such macrostructures require suitable loading and location of the catalytic moieties, as well as a good match between the hydrophobic character of the substrate and the polymer core.

In this study, triphenylphosphine(TPP)-functionalized core cross-linked micelles (TPP@CCM) were synthetized by a one-pot emulsion polymerization mediated by the reversible addition–fragmentation chain transfer (RAFT) technique, wherein the metal complex is located on the hydrophobic part of the polymer flexible arms. The method also allows great flexibility regarding the density of phosphine functions, their distribution within the object, the size of the core, and that of the hydrophilic layer. Our earlier contribution [13] has detailed the synthesis and characterization of these core–shell polymers and has provided indication of rapid mass transport of organic compounds across the hydrophilic barrier and into the hydrophobic core. It also proved them to be convenient ligands for the biphasic rhodium-catalyzed hydroformylation of 1-octene. The present paper gives a fuller and more detailed account of the catalytic results obtained varying different reaction parameters, such as catalyst/ligand concentration, temperature, P/Rh ratio, as well as the density of phosphine within the objects and the molar mass of the hydrophobic segment, and discusses the driving mechanisms.

2. Materials and methods

2.1. Materials

$[Rh(acac)(CO)_2]$ (99%, Alfa Aesar), 1-octene (99+%, Acros), *n*-nonanal (>97%, Alfa Aesar), *n*-decanal (>96%, Alfa Aesar), and anisole (99.0%, Fluka) were used as received. Carbon monoxide and dihydrogen were obtained from Linde Gas. Syngas was prepared by introducing equimolar amounts of CO and H_2 into a monitored gas reservoir feeding the autoclave reactor at constant pressure. The reference core cross-linked micelle used for the parametric reaction study was prepared as described in our previous contribution [13] and stored under an inert atmosphere.

Fig. 1 exhibits the detailed structure of the TPP@CCM made by convergent synthesis in water. The thin hydrophilic shell (degree of polymerization (DP) = 30) was formed by RAFT copolymerization of methacrylic acid and poly(ethylene oxide) methyl ether methacrylate. The subsequent hydrophobic part consisted of a styrene (S)/4-diphenylphosphinostyrene (DPPS) copolymer, with 300 units and a DPPS:S ratio of 1:9. The resulting amphiphilic block copolymers self-assembled into ca. 70 nm micelles in water. Addition of (di(ethylene glycol) dimethacrylate) (DEGDMA) cross-linker, together with additional styrene in a DEGDMA/S ratio of 1:9, allowed generating the TPP@CCMs as a concentrated latex suspension (27.3% solid content), containing 0.128 mol L^{-1} of P. Slightly modified versions of the TPP@CCMs have now been synthesized by the same procedure with either longer hydrophobic chains (DP = 500) and the same DPPS:S ratio (1:9) or with the same DP for the hydrophobic chain (300) but different DPPS:S ratios (1:19 and 1:3). See the Supporting Information for the synthesis and characterization details.

2.2. Experimental procedure

2.2.1. Biphasic hydroformylation

A Hastelloy C276 autoclave equipped with a gas-inducing stirrer was used for the hydroformylation experiments. The volumetric ratio of organic to aqueous (including the TPP@CCM latex) phases was set to 3:1 (prior to swelling) for a total volume of 0.1 L. The organic phase consisted of a mixture of 1-octene (1.1 kmol $m^{-3}_{\varphi org}$) and *n*-decanal to mimic the conditions within a continuous stirred tank reactor, where the out-flowing organic phase stream should be mainly constituted of C9 aldehydes, while allowing precise quantification of these products.

2.2.1.1. Standard reaction tests. First, Milli-Q water was introduced into a Schlenk tube and deoxygenated by nitrogen bubbling. The required quantity of TPP@CCM latex (according to desired P content) was added through a nitrogen-purged syringe, followed by stirring for 15 min. In order to swell the hydrophobic core of the nano-objects, 3 mL of *n*-decanal was added and the resulting mixture was stirred for an additional 15 min. Then, a separate solution containing $[Rh(acac)(CO)_2]$ dissolved in 3 mL of *n*-decanal was added through a Teflon cannula, and the resulting mixture was stirred for 5 min. This colloidal suspension was then transferred into the autoclave, followed by the addition of the remaining *n*-decanal (56 mL) and 1-octene (81.6 mmol). The reactor was purged three times with 15 bar of nitrogen, checked for leak under N_2 pressure, and then purged four times with 15 bar of syngas (about 25 min for the whole procedure). It was subsequently heated under low syngas pressure (2 bar) and slow stirring speed

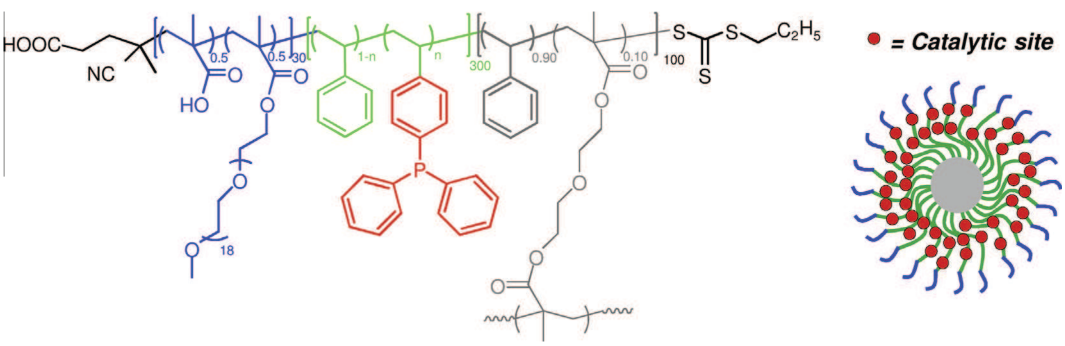

Fig. 1. Structure of the reference core cross-linked micelle (TPP@CCM), from Zhang et al. [13].

(300 rpm, well under gas self-induction) to hinder significant gas dissolution and the start of the reaction. When the desired reaction temperature was achieved (after about half an hour), stirring was stopped and the autoclave was pressurized and constantly fed with syngas at the desired pressure (20 bar). A sample was withdrawn to evaluate the amount of products formed during the heating procedure. Then, the data acquisition was started, and the stirring speed was set to 1200 rpm. Both temperature and pressure of the reactor and the gas ballast were recorded online on a computer at a rate of 1 Hz. The instantaneous reaction rate was measured from the syngas consumption. After a few hours of reaction, a final sample of organic phase was taken for the chromatographic analysis. Acquisition and heating were stopped, and the autoclave was cooled slowly at low stirring speed (200 rpm). Once the autoclave was cold, stirring was stopped and the reactor was depressurized and purged four times with nitrogen. The whole reaction mixture was let overnight for settling under nitrogen atmosphere. Finally, the content of the autoclave was then taken out and separated. Rhodium leaching in the organic phase was measured by ICP/MS (cf. Section 2.2.2).

2.2.1.2. Recycling of the catalytic phase. To perform recycling tests, the procedure was as described above, except that after cooling the reactor was kept under 2 bar of syngas and, after overnight settling, only the organic phase was withdrawn through a pipe placed above the interface with the help of the internal syngas pressure. Then, after venting the residual pressure, fresh 1-octene (81.6 mmol) and *n*-decanal (for a total volume of ca. 50 mL, corresponding to the withdrawn amount) were introduced into the autoclave through a dropping vessel pressurized with nitrogen. The reactor was subsequently purged four times with 15 bar of syngas. Heating period and reaction then proceeded as usual.

2.2.2. Analyses of the organic phase

2.2.2.1. Gas chromatography (GC). The reactant and product concentrations were measured on a Thermo Fisher Trace GC 2000 chromatograph equipped with a CB-CP WAX 52 capillary column (25 m $\times$ 0.25 mm; 0.2 µm film thickness) and a flame ionization detector (FID), using helium as carrier gas. A precise quantity of anisole (internal standard) was added before dilution with diethyl ether. The peak assignment was assisted by a separate GC/MS analysis.

2.2.2.2. High resolution inductively coupled plasma mass spectrometry (ICP/MS). The rhodium catalyst leaching in the organic phase was quantified by high resolution ICP/MS on a XR Thermo Scientific Element. For the sample preparation, the recovered organic phase was diluted into water using a 10^5 volumetric dilution factor, high enough to insure complete dissolution. In practice, a 1-L volumetric flask was filled at $\sim$2/3 with Milli-Q water, then 10 µL of the organic product phase were introduced using a Gilson P20 precision pipette. Borders were rinsed and the flask was introduced into an ultrasound bath for 30 min. The solution was left overnight and the dilution was then completed with Milli-Q water to the 1 L mark. Standards were prepared using [Rh(acac)(CO)$_2$] dissolved in *n*-decanal, attaining Rh concentrations in aqueous solution in the 1–1000 ppt range. The relative standard deviation on the measurements was less than 5%.

3. Results

3.1. Proof of concept: activity and stability of the reference TPP@CCM

The core cross-linked micelle depicted in Fig. 1 was first tested under the following conditions of biphasic hydroformylation: 1-octene/Rh = 500, P/Rh = 4, 90 °C, 20 bar of syngas, and a stirring rate of 1200 rpm, further referred to as the "standard conditions". The pH of the aqueous phase was not adjusted, and a value of 4.3 was measured after the reaction.

As generally observed with usual convenient ligands based on triphenylphosphine, no hydrogenation and low isomerization (about 5%) were observed with the functionalized CCM, the main products being C9 aldehydes (about 90% yield after 3 h), mostly *n*-nonanal and its branched isomer, 2-methyloctanal. Conversely, the phosphine-free CCM gave very similar results as the homogeneous reaction without any ligand: after 4 h of reaction under standard conditions (except no P), and the aldehyde yield was 15% (*vs.* 23% for the homogeneous ligand-free process), while the internal octenes accounted for 35% of the initial substrate charge. This demonstrated that only the polymer-linked phosphine ligand can form the active complex with rhodium.

As shown in Table 1, the TOF obtained with the reference TPP@CCM was rather high (about 500 h^{-1}, see *entries 1 and 2*) confirming that 1-octene can easily enter the functionalized hydrophobic core of the polymer despite the hydrophilic shell [13]. The measured linear to branched aldehyde regioselectivity (l/b) was up to 5.0. For comparison, the homogeneous reaction performed with a star polymer made of Boltorn core and S/DPPS arms yielded TOF up to 1030 h^{-1} and l/b ratio between 4.0 and 5.6 under similar operating conditions (90 °C, 20 bar of syngas and 1.0 M of 1-octene) [20]. The uptake of the organic phase by the nano-objects was confirmed from the weight gain of the aqueous phase. The rhodium loss in the organic phase accounted for about 1% of the amount introduced. A subsequent homogeneous hydroformylation with the recovered organic phase, mixed with fresh 1-octene, led to negligible reaction rate (less than $5 \cdot 10^{-6}$ kmol $m^{-3}_{\varphi org}$ s^{-1}).

An additional proof of concept was performed by addition of a stronger water-soluble ligand (sulfoxantphos) to the latex aqueous phase to extract the rhodium initially coordinated to the CCM phosphines into the bulk of the aqueous phase. This experiment resulted in reaction inhibition (cf. [13], recalled in *entry 3*), thus excluding any interfacial catalysis mechanism [13]. This is opposite

Table 1
First results of Rh/TPP@CCM complex for the biphasic 1-octene hydroformylation.[a]

Entry	Ligand	Run	Initial rate[b] (kmol $m_{\varphi aq}^{-3}$ s^{-1})	TOF_{max}[b] (h^{-1})	l/b[c] (–)	Leaching[d] $[Rh]_{\varphi org}$ (ppm)
1	Reference TPP@CCM (10% DPPS)	Original	$8.5 \cdot 10^{-4}$	473	4.4	2.5
1r1		1st recycle	$9.8 \cdot 10^{-4}$	541	3.9	2.7
1r2		2nd recycle	$9.4 \cdot 10^{-4}$	520	3.4	2.1
1r3		3rd recycle	$8.2 \cdot 10^{-4}$	457	3.2	1.7
1r4		4th recycle	$7.3 \cdot 10^{-4}$	402	3.6	1.7
2[e]		Repetition with fresh catalyst	$8.0 \cdot 10^{-4}$	441	5.0	2.0
3[e]	Reference TPP@CCM + sulfoxantphos[f]		$2.3 \cdot 10^{-5}$	13	–	0.1

[a] Standard conditions: $[Rh(acac)(CO)_2] = 6.5 \cdot 10^{-3}$ kmol $m_{\varphi aq}^{-3}$, [1-octene] = 1.1 kmol $m_{\varphi org}^{-3}$, P/Rh = 4 (based on P contained in TPP@CCM), $V_{\varphi org}$ = 75 mL (total volume of 1-octene + *n*-decanal), $V_{\varphi aq}$ = 25 mL (water + 1.4 g TPP@CCM, without swelling), T = 363 K, P_{syngas} = 20 bar (CO/H_2 = 1), ω = 1200 rpm.
[b] Initial reaction rate (with respect to non-swollen aqueous phase) and corresponding turnover frequency calculated from the syngas consumption during the first 5 min following gas absorption.
[c] Linear to branched aldehyde ratio determined from the GC/FID analysis of the final sample.
[d] Rh concentration in the organic phase measured by ICP/MS.
[e] Recalled from Zhang et al. [13].
[f] [Sulfoxantphos] = 0.033 kmol $m_{\varphi aq}^{-3}$ (sulfoxantphos/Rh = 5).

to what was reported with cationic surfactants [21] or polymer lattices [22] and should result from the lack of electrostatic interaction between the hydrophilic shell and the water-soluble catalytic complex. This result clearly shows that the reaction can only occur in the core of the TPP@CCM. The only role of the CCM shell is thus to confine the objects within the aqueous phase, yet allowing in and out migration of species according to their respective affinity, while catalysis actually occurs within the hydrophobic microenvironment combining catalyst and substrate.

The catalytic system stability was assessed through four successive recycles of the catalytic phase (*entries 1r1 to 1r4* of Table 1). As explained in the experimental procedure, the catalytic phase was always kept under syngas atmosphere during these recycles, but it was previously shown that its exposure to air during a few days did not result in extensive deactivation [13]. Confirming our previous observations, the first recycle gave even higher activity than the first use, possibly because all the $[Rh(acac)(CO)_2]$ precatalyst may not be fully activated during the first run. The small decrease under further recycles might be attributed to catalyst losses during the successive samplings (a small amount of aqueous phase being unavoidably withdrawn) and because of leaching in the organic phase. The rhodium leaching seemed to plateau to ca. 1.7 ppm after 3 runs. The possible cause for this leaching will be discussed more in detail below on the basis of additional evidence. Fig. 2 exhibits the evolution of the aldehyde production calculated from the syngas consumption during these successive cycles and during a repeat experiment with fresh catalyst run under the same conditions, showing reproducibility. In accordance with the narrow dispersion of the TOF values, all these profiles are very similar. The GC/FID analysis of the organic phase sample withdrawn prior to the gas induction showed that the preliminary heating period yields up to 6 mmol of aldehyde (7% conversion) and this sampling accounted for 5–10% of the total volume of organic phase. This explains the smaller measured amount of consumed syngas relative to theory (equivalent to 81.6 mmol of aldehyde) at complete conversion.

3.2. Influence of reaction parameters using the reference TPP@CCM

After confirmation that the TPP@CCM approach provides an efficient alternative for aqueous biphasic hydroformylation catalysis, additional kinetic studies were carried out to explore the effect of different operating conditions. Given that the organic phase is the continuous phase, that H_2 and CO have greater solubility in 1-octene than in water, and that 1-octene is essentially insoluble in water, the sequence of mass transfer events is probably as follows: the gaseous reactants are transported into the continuous organic phase, and all reagents migrate toward the TPP@CCM (external mass transfer) and finally diffuse within the polymer scaffold to reach the Rh catalytic sites (internal mass transfer) to be eventually transformed into products. The different operating parameters—catalyst and ligand concentrations, stirring speed, and temperature—were varied to check for mass transfer resistance, and their effects are detailed in Table 2.

3.2.1. Catalyst concentration

A common experimental test to evaluate external mass transfer limitations is to vary the catalyst concentration. If this transfer

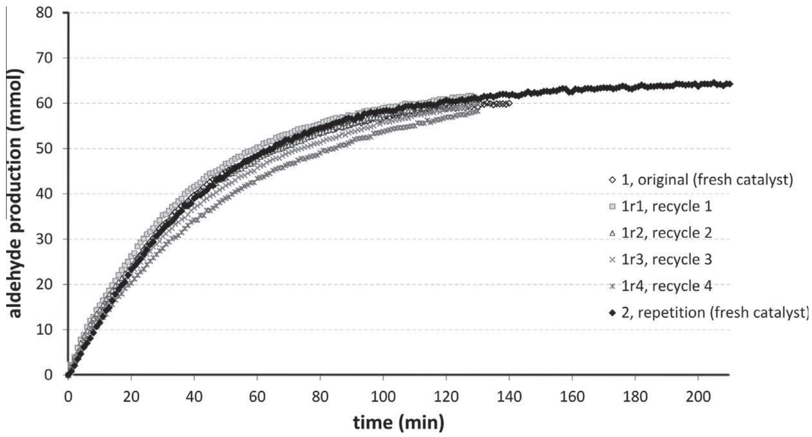

Fig. 2. Aldehyde production* during the consecutive cycles with the reference TPP@CCM in standard conditions. *Calculated from syngas consumption after gas induction (excluding the first 20 s corresponding to gas absorption).

resistance is negligible and if all Rh atoms are working in the same way, the initial reaction rate should exhibit a first-order dependence with respect to the catalyst loading (or in other words the TOF should be unchanged). Starting from standard conditions (*entry 2*), two different procedures were applied: either the concentrations of both Rh precursor and latex were varied so as to keep the same P/Rh value of 4 (*entries 4a and 4b*) or only the concentration of Rh precursor was changed while maintaining the same TPP@CCM loading (*entries 5a and 5b*). Note that these procedures might have resulted in additional but different effects. In the first approach, the metal loading of each unimolecular nano-object is the same and the activity of Rh atoms should not be modified provided that the objects do not interact with each other. However, the properties of the aqueous phase (viscosity, surface tension) are altered, and consequently, the mobility of the objects and the available aqueous-organic interface (droplet size) will also change. In the second approach, the activity of the Rh atoms might be affected as the result of variations in the P/Rh ratio (from 2 to 8). It is therefore striking that in both cases, a fourfold increase in rhodium concentration resulted only in a threefold initial rate enhancement. This suggests that a weak resistance to external mass transfer is present, probably associated to gas–liquid transport limitations. Regarding regioselectivity, the l/b ratio was slightly enhanced at the lowest concentrations of the catalytic objects but was almost unaffected by the P/Rh variation.

3.2.2. TPP@CCM concentration (at same Rh precursor concentration)

To better elucidate this effect, additional experiments were performed increasing the latex concentration, resulting in an increase of the P/Rh ratio up to 12 (*entries 6a and 6b*). No significant TOF or l/b variations were observed, showing that the aqueous phase properties did not significantly affect the physical transfers (if limiting) and that the Rh distribution within the objects played only a minor role on the whole catalytic activity for P/Rh $\geqslant$ 4. This low effect of ligand concentration differs from the usual trends in homogeneous hydroformylation, where an excess of PPh_3 with respect to the $[RhH(CO)(PPh_3)_3]$ complex led to a better selectivity toward the linear aldehyde (until a plateau was reached), with a complex effect on the reaction rate depending on the solvent nature [23]. Some homogeneous experiments were thus performed using the same composition of the organic phase and PPh_3 as a ligand, P/Rh being set at 4, 8, and 12, respectively (see details in the SI). Lower l/b ratios were achieved (less than 3), but the resulting TOF values were as high as 9000 h^{-1}. Nonetheless, no clear trends could be drawn on the effect of the P/Rh ratio, with TOF variations of less than 20% and only a slight l/b increase from 1.5 to 2.3 when increasing ligand excess.

3.2.3. Stirring speed

In order to enhance the external mass transfer (especially the gas absorption), the stirring speed was increased to 1400 and 1600 rpm (*entries 7a and 7b*). Slightly higher TOF values were observed, up to 580 h^{-1} as compared to a mean value of 460 h^{-1} at 1200 rpm, but also a significantly higher Rh leaching (about 5 times higher)—see Section 3.4. The organic phase obtained after the biphasic reaction at 1600 rpm showed little catalytic activity (about $5 \cdot 10^{-5}$ kmol $m_{\varphi org}^{-3}$ s^{-1}). Higher stirring speeds should thus be avoided in order to limit catalyst leaching with this type of CCM. During the course of the 1600 rpm reaction, the organic phase was regularly sampled and analyzed by GC in order to learn more about the time evolution of each individual reaction component. Fig. 3a exhibits the concentration–time profiles of all the reactants and products during this experiment. It confirms that isomerization was low (two different internal octenes being identified). No product other than the octenes and the aldehydes could be detected by GC, and the sum of all concentrations of these compounds yielded an excellent mass balance. Fig. 3b depicts the good agreement between the evolution of the amount of total produced aldehydes and that of the syngas consumption (as per stoichiometry). As expected from the low degree of isomerization, the l/b ratio was essentially constant during the course of the reaction.

3.2.4. Reaction temperature

Finally, the reaction was performed at two different temperatures, 343 and 353 K (*entries 8a and 8b*), in addition to the standard temperature (363 K, *entry 2*), keeping other parameters identical. Application of the Arrhenius equation yielded an activation energy of 22 kcal mol^{-1}. This value agrees well with those obtained in former studies on homogeneous and biphasic hydroformylation using monomeric ligands (PPh_3 or its trisulfonated analog) and operating in the kinetic regime: 28.0 and 13.7 kcal mol^{-1} for 1-hexene and 1-dodecene in homogeneous system [24,25], 15.7 and 19.7 kcal mol^{-1} for 1-octene and 1-dodecene in biphasic aqueous system [26,27].

This high activation energy indicates that not only the exchange of reactants/products between the continuous organic phase and the nanoreactors but also their diffusion within the TPP@CCM structure was rapid.

3.3. Comparison between different macromolecular architectures

Table 3 summarizes the performance of different macromolecular ligands derived from the reference TPP@CCM, by varying either the size of the hydrophobic block or its functionalization degree. The essential characterization details of the new polymers are provided in the Supporting Information.

3.3.1. Effect of CCM size

The test was carried out with a nano-object built in the same way as the reference TPP@CCM, except for increasing the DP of the hydrophobic chain from 300 to 500, while maintaining the

Table 2
Influence of reaction parameters on the biphasic hydroformylation of 1-octene catalyzed by the Rh/reference TPP@CCM complex.

Entry	Parameter variation from std conditions[a]	Value	Initial rate (kmol $m_{\varphi aq}^{-3}$ s^{-1})	TOF_{max} (h^{-1})	l/b (–)	$[Rh]_{\varphi org}$ (ppm)
2	No	Standard[a]	$8.0 \cdot 10^{-4}$	441	5.0	2.0
4a	[Rh] and [TPP@CCM] (P/Rh = 4)	Cata/2 (C8/Rh = 1000)	$5.1 \cdot 10^{-4}$	562	5.5	n.a.
4b		Cata × 2 (C8/Rh = 250)	$1.5 \cdot 10^{-3}$	414	4.1	n.a.
5a	[Rh] ([TPP@CCM] = const.)	[Rh]/2 (C8/Rh = 1000, P/Rh = 8)	$4.4 \cdot 10^{-4}$	484	4.6	2.7
5b		[Rh] × 2 (C8/Rh = 250, P/Rh = 2)	$1.4 \cdot 10^{-3}$	379	4.3	5.7
6a	[TPP@CCM] ([Rh] = const.)	[TPP@CCM] × 2 (P/Rh = 8)	$9.2 \cdot 10^{-4}$	507	4.4	n.a.
6b		[TPP@CCM] × 3 (P/Rh = 12)	$8.2 \cdot 10^{-4}$	454	4.8	n.a.
7a	Stirring speed	ω = 1400 rpm	$1.0 \cdot 10^{-3}$	557	3.4	6.5
7b		ω = 1600 rpm	$1.0 \cdot 10^{-3}$	579	3.5	11.6
8a	Temperature	T = 343 K	$1.3 \cdot 10^{-4}$	72	3.8	1.3
8b		T = 353 K	$3.1 \cdot 10^{-4}$	174	5.6	n.a.

[a] Standard conditions: $[Rh(acac)(CO)_2] = 6.5 \cdot 10^{-3}$ kmol $m_{\varphi aq}^{-3}$, [1-octene] = 1.1 kmol $m_{\varphi org}^{-3}$, P/Rh = 4, $V_{\varphi org}$ = 75 mL, $V_{\varphi aq}$ = 25 mL (without swelling), T = 363 K, P_{syngas} = 20 bar (CO/H_2 = 1), ω = 1200 rpm; n.a. = not available.

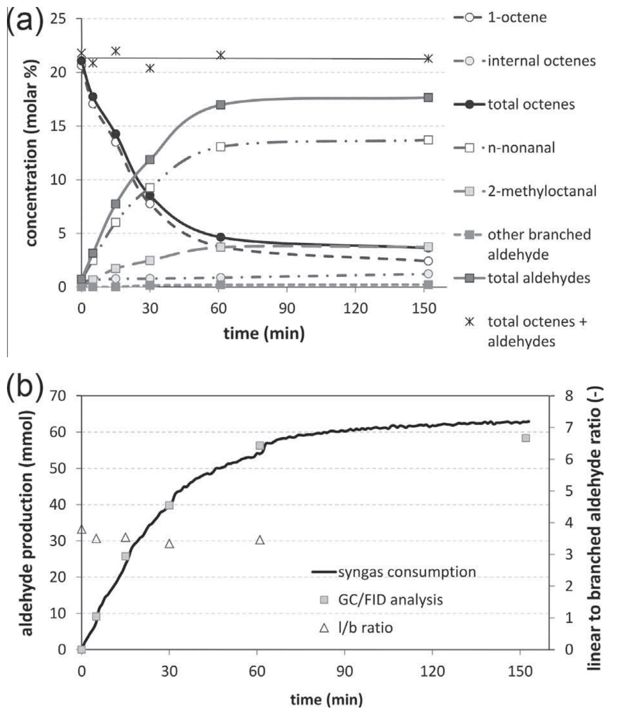

Fig. 3. Evolution of reactants and products during the reaction performed at 1600 rpm (other parameters set as per standard conditions): (a) evolution of the concentrations in the organic phase and overall mass balance, (b) comparison of the produced aldehydes from GC/FID analysis** and from syngas consumption after gas induction and time evolution of the l/b ratio. **Assuming a uniform composition of the organic phase (in the bulk and within the objects).

same DPPS:S ratio of 1:9. The initial reaction rate and l/b ratio were essentially unaffected by this increase in polymerization degree (*entry 9*), confirming that internal diffusion within the objects is not rate-limiting. Note, however, that leaching is reduced.

3.3.2. Effect of functionalization degree

To investigate the influence of the phosphine density within the polymer, two other TPP@CCMs were synthetized using DPPS:S ratios of 1:19 and 1:3 (see Supporting Information) and evaluated under standard conditions (*entries 10 and 11a*). The higher the functionalization degree of the hydrophobic core, the lower the resulting reaction rate. The l/b ratio increased upon rising the P concentration in the polymer core from 5% to 10% molar of the DPPS co-monomer, implying a possible shift to catalytic species with a higher number of coordinated phosphine ligands as these are less active and more regioselective [28]. However, a subsequent increase of the DPPS co-monomer fraction from 10% to 25% molar had no further effect on the l/b ratio. With the most functionalized TPP@CCM, halving the catalyst concentration (*entry 11b*) resulted in a larger TOF increase (by 45%) than for the reference one (by 27%, *cf. entries 2* and *4a* in Table 2). Thus, additional mass transfer limitations could be also hypothesized. Nonetheless, the temperature effect was found as strong with this ligand (*entry 11c*), discarding such an explanation.

A greater functionalization degree implies a smaller number of nanoreactors at given C8/Rh and P/Rh ratios, and thus a higher density of Rh within the objects. In spite of the fact that the local Rh distribution did not apparently result in any significant activity change for the reference TPP@CCM (cf. Section 3.2.2), this might not be the case when the phosphine moieties are closer to each other: the formation of inactive dimeric Rh species could be promoted in this case as the result of the closer vicinity of the metal atoms [29]. Another possible explanation would be that some Rh centers are not accessible due to steric hindrance caused by the high phosphine density.

3.4. Consideration on the rhodium leaching

It is possible in principle to imagine two basic mechanisms leading to Rh leaching into the organic product phase: either Rh escapes the polymer support and is transported into the organic phase by available small molecules as supporting ligands, or the polymer nanoreactor is partly transferred to the lipophilic phase during the catalytic procedure. On the basis of the known coordination chemistry of rhodium(I), leaching by rhodium extraction from the nanoreactor does not appear as a plausible explanation. Indeed, in order to extract the catalytically active hydride species from the polymer, the polymer-anchored TPP would have to be exchanged by another ligand available in the catalytic mixture. However, the only available donors are hard oxygen-based molecules (water, *n*-nonanal)—with much less affinity for Rh^I than the softer TPP—and CO. However, $[RhH(CO)_4]$ is a very elusive compound which could be observed (in the absence of TPP) only in small equilibrium amounts with $[Rh_4(CO)_{12}]$ and H_2 under a high pressure of H_2 and CO [30]. Hence, although Rh escape from the nanoreactor cannot be completely excluded at this stage, we assume that the metal is partially lost into the organic phase together with the polymer. In order to find conclusive evidence in support of this proposition, we attempted to carry out an ICP/MS analysis of phosphorus in the product phase. This measurement, however, turned out inconclusive because of some interferences due to the presence of *n*-decanal. Thus, we turned to a DLS analysis of the organic phase.

We were particularly interested in analyzing the three organic phases recovered after the experiments run with different stirring speed (*entries* 2, 7a and 7b in Table 2), because of the prominent effect that this speed had on leaching. The DLS analysis results (see Fig. 4) show the presence of nano-objects, the size of which is comparable or greater than that of the CCMs in the starting latex (79 nm/0.18 in water, 175 nm/0.28 in THF) [13]. Incidentally, the absence of smaller size particles also shows that stirring has no destructive mechanical effect on the CCM. It is interesting to note that the size of the nano-objects increases with agitation speed.

Table 3
Influence of the macroligand architecture on its performance in the biphasic 1-octene hydroformylation.

Entry	Investigated ligand	Operating conditions	Initial rate (kmol $m_{\varphi aq}^{-3}$ s^{-1})	TOF_{max} (h^{-1})	l/b (–)	$[Rh]_{\varphi org}$ (ppm)
2	Reference TPP@CCM	Standard[a]	$8.0 \cdot 10^{-4}$	441	5.0	2.0
9	TPP@CCM with $DP_{P(S\text{-}co\text{-}DPPS)}$ = 500	Standard	$8.0 \cdot 10^{-4}$	442	4.1	1.4
10	TPP@CCM with DPPS:S = 1:19	Standard	$1.3 \cdot 10^{-3}$	695	3.3	1.8
11a	TPP@CCM with DPPS:S = 1:3	Standard	$3.5 \cdot 10^{-4}$	191	4.7	1.4
11b		Std, except cata/2 (C8/Rh = 1000)	$2.5 \cdot 10^{-4}$	278	4.1	3.3
11c		Std, except T = 343 K	$4.0 \cdot 10^{-5}$	22	4.9	n.a.

[a] Standard conditions: $[Rh(acac)(CO)_2] = 6.5 \cdot 10^{-3}$ kmol $m_{\varphi aq}^{-3}$, [1-octene] = 1.1 kmol $m_{\varphi org}^{-3}$, P/Rh = 4, $V_{\varphi org}$ = 75 mL, $V_{\varphi aq}$ = 25 mL (without swelling), T = 363 K, P_{syngas} = 20 bar (CO/H_2 = 1), ω = 1200 rpm; n.a. = not available.

For the lower speed (1200 rpm, solid line), the D_z/PDI values (90 nm/0.34) are quite comparable with those of the original latex. The small increase in size can be attributed to slight core swelling by the organic medium, which is less prominent for *n*-decanal than for THF. Indeed, *n*-decanal was previously shown by a ^{1}H NMR analysis to have a small swelling power for the CCM at room temperature [13]. For the intermediate speed (1400 rpm, dashed line), the distribution remains narrow but the average size is increased (123 nm/0.18). Finally, at the highest speed (1600 rpm, dotted line), a bimodal size distribution is observed with the smaller mode centered at ca. 100 nm and the larger one at 300–400 nm.

The transport of nano-objects to the organic phase was confirmed by control experiments run by mixing the latex, either with or without rhodium, and *n*-decanal in the same proportions as in the catalytic experiment and vigorously stirring the mixture for the same time period as the catalytic run (2.5 h) and at the same temperature (90 °C). In the absence of rhodium, strong scattering resulted from the organic phase measured immediately after contact, yielding a broad particle-size distribution (PSD) with D_z = 283 nm (PDI = 0.33) which extended to more than 1 μm (Fig. 5a, solid curve). After 1 week standing at room temperature (Fig. 5a, dashed curve), the PSD shifted to smaller dimensions (D_z = 186 nm; PDI = 0.10) and became narrower. Hence, agglomerates were incontestably formed and transferred to the organic phase at high temperature, but they subsequently and slowly evolved toward monodispersed swollen particles upon cooling. Unfortunately, the DLS experiment does not provide quantitative information on the CCM concentration in the organic phase, and thus, it is not possible to extract a value for the partition coefficient, but a slight solubility of the TPP@CCM in decanal is qualitatively confirmed. The scenario was different when the polymer transport control experiment was carried out for the latex containing the Rh precatalyst [Rh(acac)(CO)$_2$] (P/Rh = 4). This time, the DLS signal of the freshly recovered *n*-decanal solution indicated a bimodal distribution, a minor one centered at slightly above 100 nm and a major one centered at ca. 650 nm, see Fig. 5b, solid curve. Upon standing for one week at room temperature, a slight shrinkage in average size was observed as expected from solvent release upon cooling, but the major distribution clearly persisted, see dashed curve in Fig. 5b. This bimodal pattern is similar to that observed after the catalytic experiment at high stirring. Note that the DLS experiments on the recovered organic phases were carried out several months after catalysis. In addition, prolonged heating (several hours) of the [Rh(acac)(CO)$_2$]/TPP@CCM latex at the reflux temperature resulted in precipitation of the polymer as an orange solid, which could no longer be dispersed in the aqueous phase. Quite evidently, the presence of rhodium favors the formation of stable aggregates that appear to be extracted into the organic phase more readily than the non-aggregated CCMs. A tentative explanation of this phenomenon is cross-linking of different poly-

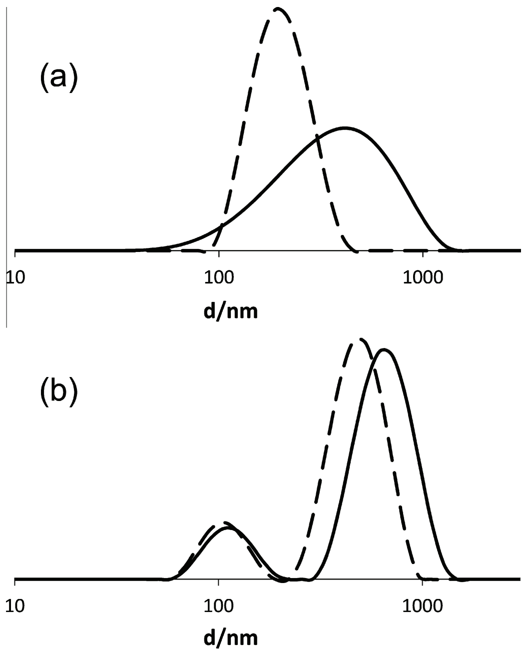

Fig. 5. DLS analysis of the recovered organic phase after stirring the TPP@CCM with *n*-decanal for 2.5 h at 90 °C (measurements carried out at room temperature): (a) without Rh and (b) with Rh (P/Rh = 4). In both cases, the solid curve was recorded immediately after recovery; the dashed curve was recorded after one week standing at room temperature.

mer cores. Indeed, [Rh(acac)(CO)$_2$] is known to replace only one CO ligand upon interaction with triphenylphosphine at room temperature to yield [Rh(acac)(CO)(TPP)] [31], but heating induces also the exchange of the second CO ligand to yield [Rh(acac)(TPP)$_2$] [32]. Therefore, the same Rh atom has the possibility to be coordinated by two TPP ligands from two different CCM cores. Note that when the control experiment was performed at room temperature, no particles were detected in the organic phase. In the catalytic reaction, the metal complex is activated by syngas and transformed to a [RhH(CO)$_n$(TPP)$_m$] species which, in the presence of a high CO pressure, probably favors the complex with $m = 1$ and therefore limits the extent of inter-particle cross-linking. While a complete understanding of the physical changes induced by the agitation to the nano-objects requires additional experiments, these preliminary results allow us to deduce that aggregation of CCMs occurs, one possible mechanism being related to inter-particle cross-linking through coordination of TPP ligands from different particle cores to the same Rh atom, that this phenomenon is favoured by heating and by a stronger agitation speed, and that the result of this aggregation is a greater extent of polymer transport into the organic phase.

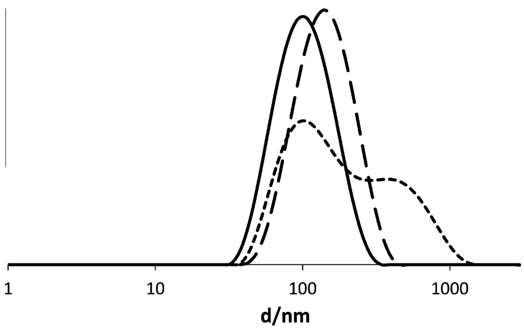

Fig. 4. DLS analysis of the recovered organic phase after the catalytic runs 2, 7a and 7b in Table 2. Stirring speed (rpm): 1200 (solid), 1400 (dashed), and 1600 (dotted).

4. Conclusions

Tailored catalytic nanoreactors for biphasic catalysis have shown promising results in the hydroformylation of 1-octene: high activity, low isomerization and good stability (Rh leaching of a few ppm), and recyclability. Independent variations of several process parameters have led to the same conclusion of an efficient transfer of the substrates into and within the nanoreactor hydrophobic core. Nevertheless, a moderate mass transfer limitation occurs for high rhodium concentrations, which is more likely due to rhodium interactions than to interfacial or internal mass transfer. A preliminary design study provided clues toward their optimization: a lower degree of functionalization leads to higher TOF. A kinetic modeling and the mass transfer mechanism are under investigation, which goes through the analysis of the microenvironment composition. Finally, leaching appears related to a particle aggregation phenomenon probably through particle cross-linking which appears accentuated by more vigorous stirring. In order to reduce or completely eliminate this phenomenon, we are currently investigating other polymer architectures that differ by either core cross-linking or shell chemical nature. The results of these investigations will be published in due course.

Acknowledgments

This work was carried out with the financial support of the Agence Nationale de la Recherche (ANR) under the Biphasnanocat Project (ANR-11-BS07-025-01). We thank J.L. Labat, I. Coghe, and M.L. Pern (LGC) for their technical support and F. Candaudap (GET Toulouse) for ICP/MS analyses.

Appendix A. Supplementary material

Supplementary data associated with this article can be found, in the online version, at http://dx.doi.org/10.1016/j.jcat.2015.01.009.

References

[1] C.R. Mathison, D.J. Cole-Hamilton, in: D.J. Cole-Hamilton, R.P. Tooze (Eds.), Recovery and Recycling, Chemistry and Process Design, Springer, Doedrecht, 2006, p. 145.
[2] M. Earle, P. Wasserscheid, P. Schulz, H. Olivier-Bourbigou, F. Favre, M. Vaultier, A. Kirschning, V. Singh, A. Riisager, R. Fehrmann, S. Kuhlmann, in: P. Wasserscheid, T. Welton (Eds.), Ionic Liquids in Synthesis, second ed., Wiley-VCH, Weinheim, 2008, p. 265.
[3] S. Doherty, in: C. Hardacre, V. Parvulescu (Eds.), Catalysis in Ionic Liquids: From Catalyst Synthesis to Application, Royal Society of Chemistry, 2014, p. 44.
[4] H. Olivier-Bourbigou, F. Favre, A. Forestière, F. Hugues, Handbook of Green Chemistry 1 (5) (2010) 101.
[5] I. Hablot, J. Jenck, G. Casamatta, H. Delmas, Chem. Eng. Sci. 47 (1992) 2689.
[6] F. Monteil, R. Queau, P. Kalck, J. Organomet. Chem. 480 (1994) 177.
[7] P. Purwanto, H. Delmas, Catal. Today 24 (1995) 135.
[8] E. Monflier, S. Tilloy, G. Fremy, Y. Castanet, A. Mortreux, Tetrahedron Lett. 36 (1995) 9481.
[9] M. Ferreira, F.X. Legrand, C. Machut, H. Bricout, S. Tilloy, E. Monflier, Dalton Trans. 41 (2012) 8643.
[10] J. Boulanger, A. Ponchel, H. Bricout, F. Hapiot, E. Monflier, Eur. J. Lipid Sci. Technol. 114 (2012) 1439.
[11] N. Six, A. Guerriero, D. Landy, M. Peruzzini, L. Gonsalvi, F. Hapiot, E. Monflier, Catal. Sci. Technol. 1 (2011) 1347.
[12] L. Obrecht, P.C.J. Kamer, W. Laan, Catal. Sci. Technol. 3 (2013) 541.
[13] X. Zhang, A.F. Cardozo, S. Chen, W. Zhang, C. Julcour, M. Lansalot, J.F. Blanco, F. Gayet, H. Delmas, B. Charleux, E. Manoury, F. D'Agosto, R. Poli, Chem. Eur. J. (2014), http://dxdoi.org/10.1002/chem03819. Published online: 03.10.14.
[14] H. Mao, H. Yu, J. Chen, X. Liao, Sci. Rep. 3 (2013) 2226.
[15] A. Gong, Q. Fan, Y. Chen, H. Liu, C. Chen, F. Xi, J. Mol. Catal. A 159 (2000) 225.
[16] T. Terashima, M. Ouchi, T. Ando, M. Kamigaito, M. Sawamoto, Macromolecules 40 (2007) 3581.
[17] T. Terashima, M. Ouchi, T. Ando, M. Sawamoto, Polym. J. 43 (2011) 770.
[18] Y. Liu, Y. Wang, Y. Wang, J. Lu, V. Piñón, M. Weck, J. Am. Chem. Soc. 133 (2011) 14260.
[19] A. Lu, D. Moatsou, D.A. Longbottomb, R.K. O'Reilly, Chem. Sci. 4 (2013) 965.
[20] A.F. Cardozo, E. Manoury, C. Julcour, J.F. Blanco, H. Delmas, F. Gayet, R. Poli, Dalton Trans. 42 (2013) 9148.
[21] H. Chen, Y. Li, J. Chen, P. Cheng, Y. He, X. Li, J. Mol. Catal. A 149 (1999) 1.
[22] H. Nowothnick, A. Rost, T. Hamerla, R. Schomäcker, C. Müller, D. Vogt, Catal. Sci. Technol. 3 (2013) 600.
[23] R.M. Deshpande, B.M. Bhanage, S.S. Divekar, R.V. Chaudhari, J. Mol. Catal. 78 (1993) L37.
[24] R.M. Deshpande, R.V. Chaudhari, Ind. Eng. Chem. Res. 27 (1988) 1996.
[25] B.M. Bhanage, S.S. Divekar, R.M. Deshpande, R.V. Chaudhari, J. Mol. Catal. A 115 (1997) 247.
[26] R.M. Deshpande, Purwanto, H. Delmas, R.V. Chaudhari, Ind. Eng. Chem. Res. 35 (1996) 3927.
[27] Y.Z. Li, H. Chen, J.R. Chen, P.M. Cheng, J.Y. Hu, X.J. Li, Chinese J. Chem. 19 (2001) 58.
[28] P.W.N.M. van Leeuwen, Homogeneous Catalysis: Understanding the Art, Springer, 2005.
[29] K.S. Ro, S.I. Woo, Appl. Catal. 69 (1991) 169.
[30] C. Li, E. Widjaja, W. Chew, M. Garland, Angew. Chem. Int. Ed. 41 (2002) 3786.
[31] F. Bonati, G. Wilkinson, J. Chem. Soc. (1964) 3156
[32] D.M. Barlex, M.J. Hacker, R.D.W. Kemmitt, J. Organomet. Chem. 43 (1972) 425.